Molecular Biology of the Cell
Vol. 20, 4070–4082, September 15, 2009

Guanine Nucleotide Exchange Factor-H1 Regulates Cell Migration via Localized Activation of RhoA at the Leading Edge

Perihan Nalbant,*† Yuan-Chen Chang,*‡ Jörg Birkenfeld,*§ Zee-Fen Chang,‡ and Gary M. Bokoch*

*Departments of Immunology and Microbial Science, and Cell Biology, The Scripps Research Institute, La Jolla, CA 92037; †Department of Molecular Cell Biology, Center for Medical Biotechnology, University of Duisburg-Essen, 45117 Essen, Germany; ‡Institute of Biochemistry and Molecular Biology, College of Medicine, National Taiwan University, Taipei 100, Taiwan

Submitted January 14, 2009; Revised July 1, 2009; Accepted July 9, 2009
Monitoring Editor: Paul Forscher

Cell migration involves the cooperative reorganization of the actin and microtubule cytoskeletons, as well as the turnover of cell–substrate adhesions, under the control of Rho family GTPases. RhoA is activated at the leading edge of motile cells by unknown mechanisms to control actin stress fiber assembly, contractility, and focal adhesion dynamics. The microtubule-associated guanine nucleotide exchange factor (GEF)-H1 activates RhoA when released from microtubules to initiate a RhoA/Rho kinase/myosin light chain signaling pathway that regulates cellular contractility. However, the contributions of activated GEF-H1 to coordination of cytoskeletal dynamics during cell migration are unknown. We show that small interfering RNA-induced GEF-H1 depletion leads to decreased HeLa cell directional migration due to the loss of the Rho exchange activity of GEF-H1. Analysis of RhoA activity by using a live cell biosensor revealed that GEF-H1 controls localized activation of RhoA at the leading edge. The loss of GEF-H1 is associated with altered leading edge actin dynamics, as well as increased focal adhesion lifetimes. Tyrosine phosphorylation of focal adhesion kinase and paxillin at residues critical for the regulation of focal adhesion dynamics was diminished in the absence of GEF-H1/RhoA signaling. This study establishes GEF-H1 as a critical organizer of key structural and signaling components of cell migration through the localized regulation of RhoA activity at the cell leading edge.

INTRODUCTION

Cell migration plays key roles in the regulation of such critical processes as wound healing, neuronal development, and immune responsiveness. It is now well established that the Rho GTPase proteins RhoA, Rac, and Cdc42 regulate cell migration through the precise spatial and temporal coordination of dynamic actin-based structures, such as the protrusive lamellipodia found at the leading edge of migrating cells. In addition, Rho GTPases regulate integrin-based adhesion sites to control cell attachment, spreading, and detachment (for reviews, see Hall, 1998; Ridley, 2001; Etienne-Manneville *et al*., 2002). Whereas Rac and Cdc42 promote nascent focal contact formation in dynamic protrusions at the leading edge, RhoA mediates contractile actin stress fiber assembly, a process important for the maturation of focal contacts into larger focal adhesions (FAs). A strong correlation exists between the traction force generated by cell–substratum adhesion and the growth and turnover of focal adhesions during cell migration (for review, see Bershadsky *et al*., 2003). The diversity of Rho GTPase signaling during migration is thought to ensure a fine balance between cell adhesion and protrusion that is critical for efficient and controlled translocation (for review, see Ridley *et al*., 2003).

A key event for the spatiotemporal regulation of motility is the localized activation of Rho GTPases. Earlier studies had linked Rac1 activity to protrusion of the leading edge, whereas Rho activity had been shown to be required for contractile activity that supported retraction of the cell body and trailing tail (for reviews, see Etienne-Manneville, 2002; Ridley, 2001; Worthylake and Burridge, 2001). These observations and others supported a simple view of Rac activation primarily at the cell anterior, with Rho activation at the cell posterior. However, the activities of Rho proteins in migrating cells have recently been visualized using real-time fluorescent biosensors, and the highest levels of activity observed with Rac1, Cdc42, and RhoA have all been predominantly in the dynamic leading edge (Kraynov *et al*., 2000; Gardiner *et al*., 2002; Nalbant *et al*., 2004; Pertz *et al*., 2006). Interestingly, Cdc42 and Rac1 were activated ~2 μm behind the leading edge during cell protrusion, and their activity decreased in a broad gradient toward the cell interior (Machacek *et al*., 2009). In clear contrast, RhoA activity unexpectedly displayed a peak adjacent to the very cell edge synchronous with edge advancement, whereas there was a delay in Cdc42 and Rac1 activation relative to the initiation of protrusion (Pertz *et al*., 2006; Machacek *et al*., 2009). These data are consistent with studies demonstrating that RhoA signaling is functionally associated with leading edge extension, ruffling, and motility (Fukata *et al*., 1999; Matsumoto *et al*., 2001;

This article was published online ahead of print in *MBC in Press* (http://www.molbiolcell.org/cgi/doi/10.1091/mbc.E09–01–0041) on July 22, 2009.

Present address: §DIREVO Biotech AG, 50829 Cologne, Germany.

Address correspondence to: Gary M. Bokoch (bokoch@scripps.edu) or Perihan Nalbant (perihan.nalbant@uni-due.de).

Palazzo *et al*., 2001; Kurokawa *et al*., 2005; El-Sibai *et al*., 2008). There is very little knowledge of molecular pathways regulating localized Rho activity in migrating cells and the relevance of such signaling for coordinated cell translocation is still unclear.

Interestingly, various studies have implicated Rho GTPase-dependent cross-talk between microtubules (MTs) and the actin cytoskeleton during cell migration (for reviews, see Wittmann and Waterman-Storer, 2001; Etienne-Manneville, 2004). Coordinated actin dynamics requires an intact MT cytoskeleton, because lack of a functional microtubule lattice inhibits cell polarization and dynamics of leading edge lamellipodia (Mikhailov and Gundersen, 1998; Etienne-Manneville and Hall, 2001; Baudoin *et al*., 2008). Dynamic MTs at the leading edge of migrating cells are necessary for efficient Rac-dependent protrusive behavior, whereas in turn Rac signaling promotes MT penetration into the leading edge, suggesting a positive feedback loop (Waterman-Storer *et al*., 1999; Wittmann *et al*., 2003). Nocodazole-induced depolymerization of MTs suppresses cell protrusion, while increasing RhoA-dependent contractility and actin stress fiber formation (Danowski, 1989; Enomoto, 1996). It is therefore conceivable that during migration discrete localized Rho activities function to regulate cross-talk between these two cytoskeletal networks in a spatial and temporal manner.

Multiple guanine nucleotide exchange factors (GEFs) that activate Rho GTPases in vitro and in vivo have been identified (for review, see Rossman *et al*., 2005). The Rho-specific exchange factor GEF-H1 is of particular interest, because its catalytic activity toward RhoA is negatively regulated by MT binding (Ren *et al*., 1998; Krendel *et al*., 2002). Chang *et al*. (2008) showed that a signaling cascade composed of GEF-H1/RhoA/Rho kinase (ROCK) and myosin light chain (MLC) plays a critical role in mediating cell contractility induced by microtubule depolymerization (Chang *et al*., 2008). In addition to this direct effect on cell contractility, GEF-H1 has also been found to be a component of tight junctions and is important for the integrity of cell–cell adhesion (Benais-Pont *et al*., 2003). Although both of these processes are important in cell motility, the exact role of GEF-H1 upstream of RhoA activity in migrating cells is not known. However, a critical role for GEF-H1 in regulating RhoA activation during cleavage furrow initiation in dividing HeLa cells has been demonstrated (Birkenfeld *et al*., 2007).

Here, we investigated the effects of GEF-H1 depletion by using small interfering RNA (siRNA) technology on localized RhoA activity in the context of cell motility. GEF-H1 depletion led to aberrant localized RhoA activation in the leading edge, accompanied by reduced migration. The lack of proper actin-myosin-based contractility in the affected cells, along with decreased turnover of focal adhesions, gave rise to dramatic changes in actin and protrusion dynamics at the cell edge. Our data reveal GEF-H1 as a critical component of the locomotory machinery, coordinating multiple RhoA-dependent signaling pathways during the migration of cells.

MATERIALS AND METHODS

Reagents and Antibodies

Nocodazole was purchased from Sigma-Aldrich (St. Louis, Mo.) and was dissolved in dimethyl sulfoxide. Generation and affinity purification of the polyclonal anti-GEF-H1 antibody used in this study has been described previously (Zenke *et al*., 2004). The antibody was used at 1:1000 in immunoblots and 1:100 in immunofluorescence (IF) experiments. The following commercial antibodies were used: for immunostaining, monoclonal anti-α-tubulin (clone B-5-1-2; Sigma-Aldrich) and anti-paxillin antibodies (BD Biosciences Transduction Laboratories, Lexington, KY) at 1:1000 and 1:500 dilution, respectively. Alexa-labeled secondary antibodies (Invitrogen, Carlsbad, CA) and rhodamine-labeled phalloidin (Sigma-Aldrich) were used at 1:500 dilution.

For immunoprecipitation (IP) experiments and immunoblots, the following antibodies were used: monoclonal anti-paxillin (BD Biosciences Transduction Laboratories; 1:100), monoclonal anti-Myc (9E10, prepared in-laboratory; 1:200), monoclonal anti-actin (C4, MP Biomedicals, Solon, OH; 1:10,000), monoclonal anti-phosphotyrosine (clone 4G10, Millipore, Billerica, MA; 1:4000), monoclonal anti-focal adhesion kinase (FAK) (clone 4.47, Millipore; 1:1000), and anti-pFAK (rabbit, pY397, Invitrogen; 1:2000).

Cell Culture and RNA Interference

HeLa cells were maintained in DMEM (Invitrogen) containing 8% fetal bovine serum (FBS), 2 mM L-glutamine, 100 U/ml penicillin G, and 100 U/ml streptomycin. For RNA interference experiments, nontargeting control, GEF-H1- (siGenome, ON-Target Plus), and mDia1- [si-mDia1(K2)] targeting duplex oligonucleotides were purchased from Dharmacon RNA Technologies (Boulder, CO). The siRNA pool targeting GEF-H1 contained the following four oligonucleotides (oligos): oligo 6 (J-009883-06, 5′-GAAUUAAGAUGGAGUUGCAUU-3′), oligo 7 (J-009883-07, 5′-GUGCGGAGCAGAUGUGUAAUU-3′), oligo 8 (J-009883-08, 5′-GAAGGUAGCAGCCGUCUGUUU-3′), and oligo 9 (J-009883-09, 5′-CCACGGAACUGGCAUUACUUU-3′). The sequence of the mDia1 targeting oligonucleotide (LUJAF-000492) was 5′-GCUGGUCAGAGCCAUGGAU-3′. For the assay, ~150,000 HeLa cells grown per well of a six-well plate were transfected with control, GEF-H1 (10 nM final) or mDia1 (100 nM final) siRNA by using 4 μl of Lipofectamine 2000 (Invitrogen). At 24 h after transfection, cells were trypsinized and replated on glass coverslips, and live-cell differential interference contrast (DIC) imaging was conducted at 72 h after transfection. For assays requiring overexpression of exogenous enhanced green fluorescent protein (EGFP)-tagged proteins, cells were transfected with the appropriate constructs at 48 h after the siRNA transfection, and fluorescence imaging was then performed the next day (72 h after siRNA transfection). As control for possible off-target effects, each single oligo was tested.

DNA Constructs

EGFP-GEF-H1-wild type (WT) and EGFP-GEF-H1-(DH) constructs in the mammalian expression vector pCMV5 have been described previously (Krendel *et al*., 2002; Zenke *et al*., 2004). Mutant constructs resistant to the siRNA oligo 9 [EGFP-GEF-H1-WT^{9R} and EGFP-GEF-H1-(DH^{9R})] were generated by site-directed mutagenesis as described in Chang *et al*. (2008). The constructs encoding for EGFP-EB1 and EGFP-actin were gifts from Leif Dehmelt (TSRI). EGFP-paxillin was a gift from Clare Waterman-Storer (National Institutes of Health, Bethesda, MD). The RhoA biosensor construct for live-cell fluorescence resonance energy transfer (FRET) experiments was kindly provided by Olivier Pertz (Center for Biomedicine, University of Basel, Basel, Switzerland) and Klaus Hahn (University of North Carolina, Chapel Hill, NC). The generation of stable biosensor-expressing HeLa cell lines were described in Birkenfeld *et al*. (2007).

Migration Experiments

For two-dimensional (2D) migration studies, cells were replated on glass coverslips 24 h after siRNA transfection at high density (2×10^5/well of a six-well plate). At 72 h after transfection, a scratch was generated. After 30 min recovery time phase-contrast time-lapse movies of randomly chosen regions were imaged using a 20× objective lens and a frame rate of 1 min. Migration area was analyzed using standard image analysis tools provided by MetaMorph (Molecular Devices, Sunnyvale, CA). Three-dimensional migration was assessed using a modified Boyden chamber transwell assay with 8-μm pore filters (Millipore) coated with fibronectin (10 μg/ml; Sigma-Aldrich). At 54 h post-siRNA transfection, HeLa cells were incubated in migration medium (DMEM with 1% FBS) for 18 h and then trypsinized. Cells were resuspended in fresh migration medium and placed in the upper chamber of the filter (10^5 cells in 300 μl). The lower chamber of the transwell was filled with 400 μl of migration medium either with or without 20% FBS. After 6 h of incubation, the filters were removed and the migrating cells on the underside of the chamber were fixed using 4% paraformaldehyde. Cells were visualized by 0.1% crystal violet staining. Randomly, 10 images of each filter were captured using a 20× objective lens to calculate the number of migrated cells (n = 6 filters for each condition; n = 3 filters to determine total cell numbers). To determine the overall number of cells used for each transfection condition, additional transwell filters were used in parallel, and the number of cells in the upper side together with the number of cells in the bottom side of the chamber was counted (n = 3 filters for each condition).

Immunofluorescence and Cell Imaging

For immunofluorescence staining, cells were fixed with 4% paraformaldehyde for 20 min at 37°C, permeabilized with 0.5% Triton X-100 for 5 min at room temperature followed by blocking with 5% bovine serum albumin in phos-

phate-buffered saline (PBS) for 1 h. Specimens were incubated with the appropriate primary and secondary antibodies at the indicated dilutions.

Fluorescence and brightfield imaging was performed on a fully automated TE2000-U microscope (Nikon, Tokyo, Japan) controlled by MetaMorph software (Molecular Devices) equipped with a CoolSNAP FX camera (Roper Scientific, Trenton, NJ). Images were acquired using a 20× phase contrast or 60×/1.4 numerical aperture (NA) oil objective with appropriate filter sets. Time-lapse imaging of migrating cells was carried out in a sealed chamber at 37°C and with indicated frame rates. For fluorescence experiments, live-cell imaging medium was used (F-12 medium without phenol red [Invitrogen] supplemented with 8% FBS, 2 mM L-glutamine, and 2 mM HEPES). Image processing was performed with MetaMorph (Molecular Devices), ImageJ (http://rsb.info.gov/ij/), and Adobe Photoshop software (Adobe Systems, Mountain View, CA).

FRET Imaging of RhoA Activation in Living Cells

Localized RhoA activation was visualized using a live-cell FRET probe described previously (Pertz *et al*., 2006). HeLa cells stably expressing the RhoA probe were used for FRET activity assays (Birkenfeld *et al*., 2007). Biosensor cells were transfected with nontargeting control or GEF-H1–specific siRNA for 48–72 h. Live-cell FRET imaging was performed with multiple cells randomly selected from each population. Cyan fluorescent protein (CFP) and FRET images were acquired using a 60×/1.4 NA oil objective and the following fluorescence filter sets (Chroma Technology, Brattleboro, VT) for sensitized emission FRET assay: CFP, D436/20, D470/40; and FRET, D436/20, HQ535/30. A dichroic mirror was custom manufactured (Chroma Technology) for compatibility with all the filters named above. Cells were illuminated with a 200-W Hg lamp, and exposure times were adjusted to the expression level of the RhoA biosensor (typically 50–100 ms, with 2 × 2 binning). Image analysis was performed using MetaMorph (Molecular Devices) and ImageJ software (http://rsb.info.gov/ij/) essentially as described previously (Pertz *et al*., 2006; Birkenfeld *et al*., 2007). In brief, each image was shading corrected and background subtracted. A threshold based mask was generated and applied to each CFP and FRET image. By doing so, noise outside of the cell was eliminated. In a final step, the image representing RhoA activity was generated by dividing the processed FRET image by the corresponding CFP image. As images were acquired sequentially, the postimaging ratiometric process might generate artifacts due to motion between two acquisitions. To account for such possible artifacts a control ratio image was generated using two sequentially acquired CFP images for the ratio operation. This technique reveals maximum false positive signal originating from cell movement during the time lapse.

Paxillin Immunoprecipitation (IP) and Tyrosine Phosphorylation

Tyrosine phosphorylation of paxillin was assessed by IP and subsequent immunoblotting. At 72 h after siRNA-transfection, cells in 100 mm-diameter dishes were rinsed with ice-cold PBS and scraped off into lysis buffer (50 mM Tris-HCl, pH 7.5, 1% NP-40, 0.1% SDS, 0.25% sodium deoxycholate, 10 mM NaF, 2 mM Na_2VO_4, 5 mM $MgCl_2$, 150 mM NaCl, 1 mM dithiothreitol [DTT], 1 mM β-glycerophosphate, 1 mm phenylmethylsulfonyl fluoride[PMSF], and appropriate dilutions of the protease inhibitors leupeptin, aprotinin, and pepstatin). After syringe shearing, the insoluble debris was removed by centrifugation at 13,000 × *g* for 10 min at 4°C. Aliquots of lysates were incubated with the primary mouse anti-paxillin or anti-myc antibody for 2.5 h at 4°C, and protein A-agarose was added for additional 0.5 h. Immune complexes were washed four times in lysis buffer without SDS and sodium deoxycholate. IPs or total lysates were subjected to SDS-polyacrylamide gel electrophoresis (PAGE) for immunoblot analysis using the antibodies against phospho-Tyr (4G10), GEF-H1, and actin. IPs were confirmed by stripping the membrane of phospho-Tyr antibody and reprobing with anti-paxillin antibody. The proteins were detected by enhanced chemiluminescence according to the manufacturer's instructions.

FAK Activation

After 72 h of siRNA treatment, cells were lysed in lysis buffer (50 mM Tris-HCl, pH 7.5, 1% NP-40, 10 mM NaF, 2 mM Na_3VO_4, 5 mM $MgCl_2$, 150 mM NaCl, 1 mM EDTA, 1 mM DTT, 1 mM β-glycerophosphate, 1 mM PMSF, and appropriate dilutions of the protease inhibitors leupeptin, aprotinin, and pepstatin). Cell lysates were separated by SDS-PAGE, transferred to membranes, and subjected to Western blot to visualize pFAK (Tyr397), indicating the level of active FAK.

RESULTS

GEF-H1 Depletion Inhibits Cell Migration in a Rho-dependent Manner

GEF-H1 is a Rho-specific guanine nucleotide exchange factor that mediates cross-talk between the MT and actin cytoskeletons through the MT-dependent activation of Rho/ROCK-mediated acto-myosin-dependent contractility and stress fiber formation. Supplemental Movie 1 shows that the control HeLa cells used in these experiments were highly motile. To assess the role(s) of GEF-H1 in HeLa cell migration, we used siRNA to deplete GEF-H1. GEF-H1 knockdown was efficient, with >95% siRNA-transfected cells (Supplemental Figure S1A), and depletion of >80% of endogenous GEF-H1 routinely observed (Figure 1, A and B). Single cell analysis using immunostaining for endogenous GEF-H1, as well as expression of exogenous EGFP-tagged GEF-H1 in the presence of GEF-H1 siRNA, revealed significant decrease of GEF-H1 protein in the majority of the cells below the minimum levels detected in control cells (Supplemental Figure S1, B and C).

GEF-H1–depleted cells exhibited significantly slower migration behavior in in vitro three-dimensional migration experiments by using fibronectin-coated filters, as well as in wound healing assays (Figure 1, A and C). The magnitude of the effect was comparable in both assays, suggesting that similar pathways downstream of GEF-H1 might be affected in each scenario. The decrease in cell migration observed in the GEF-H1–depleted cells was not due to differences in cell viability (Supplemental Figure S2).

To verify that the observed migration defect was specifically caused by the depletion of GEF-H1, we cotransfected cells expressing the GEF-H1 siRNA with an siRNA-resistant mutant of EGFP-tagged wild-type GEF-H1 (EGFP-GEF-H1^{9R}). This led to increased cell migration in the in vitro scratch assay compared with the expression of an siRNA-sensitive GEF-H1-wt construct, confirming the specificity of the siRNA effects (Figure 1C). By introducing a mutation into the DH-region of this siRNA-resistant construct (EGFP-GEF-H1-DH^{9R}), we were able to test whether the catalytic exchange activity of GEF-H1 was involved in the decreased migration efficiency. Indeed, we observed that cotransfection of the inactive construct (EGFP-GEF-H1-DH^{9R}) with GEF-H1 siRNA was unable to rescue cell migration, and the migration efficiency was similar to that of the siRNA-targeted GEF-H1-wt construct. Thus, the decrease of migration efficiency upon GEF-H1 depletion is a result of the loss of GEF-H1 Rho exchange activity.

GEF-H1 Depletion Causes Aberrant RhoA Activation Dynamics at the Leading Edge

The requirement for intact Rho GEF activity of GEF-H1 for normal cell motility led us to examine the activity of its target GTPase, RhoA, during cell motility. As we had shown previously, when we measured bulk RhoA activity with an affinity-based pull-down assay, we could not detect any significant change of overall RhoA-GTP levels in cells depleted of GEF-H1 (Chang *et al*., 2008). This was perhaps not unexpected, because only a small proportion of the entire Rho GTPase protein pool might be active in cells growing in serum. Moreover, Rho activation is likely to be subjected to tight control by upstream regulators to permit highly localized signaling responses. Indeed, studies by us and others using fluorescent activation biosensors in migrating cells have shown that Rho GTPase activation is highly spatially and temporally regulated, particularly at the cell leading edge (Kraynov *et al*., 2000; Gardiner *et al*., 2002; Kurokawa *et al*., 2004; Nalbant *et al*., 2004; Pertz *et al*., 2006; Machacek *et al*., 2009). To assess whether GEF-H1 function is important for localized activation of RhoA during cell migration, we used a genetically encoded fluorescence biosensor based on FRET (Pertz *et al*., 2006). Using this probe, Pertz *et al*. (2006) previously showed that in randomly migrating mouse em-

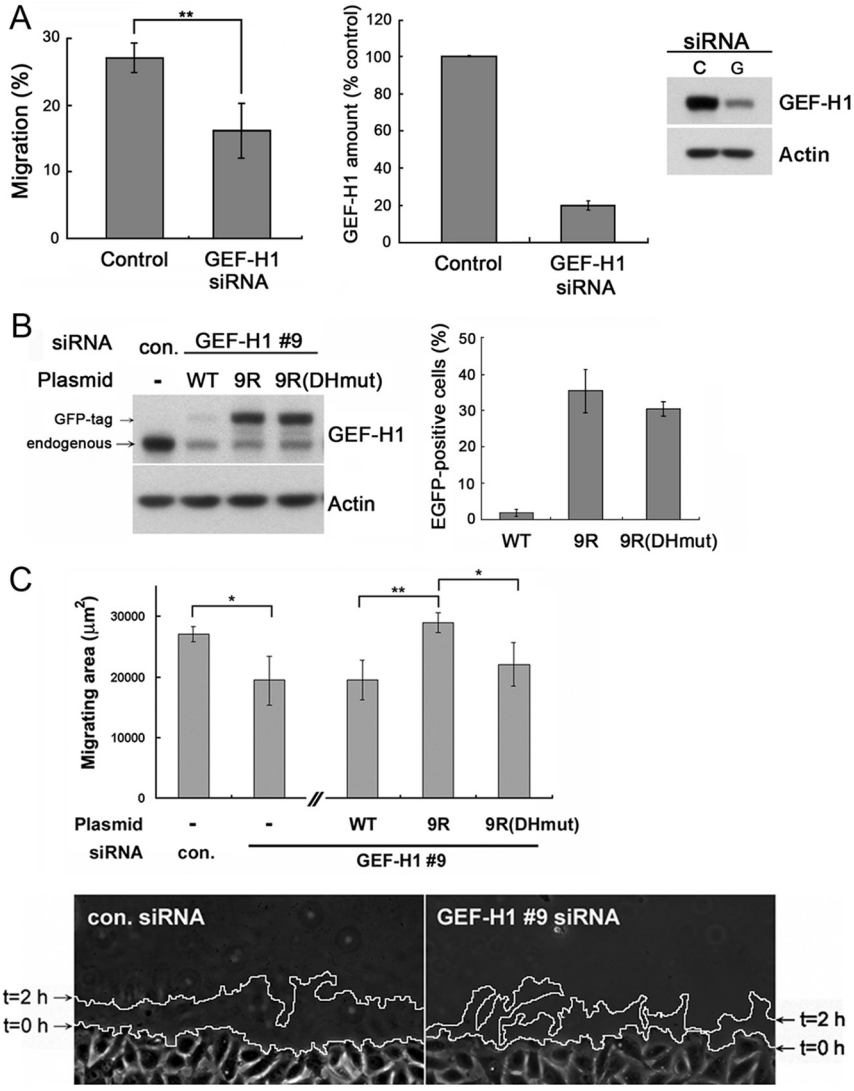

Figure 1. GEF-H1–depleted cells migrate slower. (A) Three-dimensional migration of HeLa cells is inhibited upon GEF-H1 depletion. At 72 h post-siRNA transfection, cells were either harvested for Western blotting or seeded on a 3D migration filter coated with fibronectin matrix to allow migration through the filter for 6 h. Left, percentage of migrated cells. Results are means ± SD from three independent transfection experiments. Middle, GEF-H1 protein level in control and GEF-H1 siRNA treated cells. GEF-H1 amount was quantified by Western blot using anti-GEF-H1 antibody at 72 h post-siRNA transfection. Results are means ± SD from n = 8 independent transfection experiments. Right, representative blot. See also Supplemental Figure 1 for single cell quantification. (B) Transfection of siRNA-resistant EGFP-GEF-H1 plasmids in HeLa cells. Cells were treated with control or GEF-H1-specific #9 siRNA and transfected with the indicated EGFP-GEF-H1 plasmids 48 h post-siRNA treatment. 9R and $9R^{DHmut}$ represent EGFP-GEF-H1 constructs resistant to GEF-H1-specific siRNA oligo #9. At 72 h post-siRNA transfection, cells were lysed to analyze GEF-H1 expression level by Western blot using anti-GEF-H1 antibody (left). In parallel, transfected cells were fixed to visualize EGFP fluorescence together with nuclear 4,6-diamidino-2-phenylindole staining to quantify the percentage of EGFP positive cells (right). Results are ±SD from three independent experiments. (C) In vitro wound healing of HeLa cells in 2D. At 72 h post-siRNA transfection, a scratch was generated into the confluent monolayer and cells were allowed to migrate for 2 h. Cell outlines were drawn along the wound edge at time = 0 h (imaging start) and 2 h, as indicated in the bottom panel. Migration was quantified by calculating the area between the two outlines by using MetaMorph software. Results are the means ± SD of four independent experiments. Bottom, representative migration area after 2 h of wound closure of control and GEF-H1–specific #9 siRNA-treated cells. *$p < 0.05$ and **$p < 0.01$.

bryonic fibroblasts, RhoA activity is localized to distinct zones in dynamic protrusions. A band of high RhoA activity was localized at the very distal part of the leading edge in regions where protrusions were extending. In addition, high levels of RhoA activity were found on the distal side of serum-induced membrane ruffles.

Similar to the observations by Pertz *et al*. (2006) in mouse embryonic fibroblasts, our studies of randomly migrating HeLa cells also revealed highest RhoA activity in dynamic protrusions and regions showing strong edge ruffling (Figure 2). This general overall distribution of RhoA activity was observed both in control and GEF-H1–depleted conditions (Figure 2A). Some cells also displayed high RhoA-GTP levels in their tail region, coincident with strong tail contraction. However, the latter was rather rare (only 2 of 16 control cells) and could not be assessed statistically. As observed with the affinity-based pull-down assay, when we compared the average cellular RhoA activity levels using the average RhoA FRET values in each cell, we could not detect a significant difference in cells in which GEF-H1 had been depleted (Figure 2D, top). However, when we quantified RhoA activity within 1 μm of the cell edge in membrane protrusions relative to the overall activity (Figure 2D, bottom), there was a significant decrease of ~50% in the GEF-H1–depleted cells.

To evaluate the dynamics of RhoA activation in randomly migrating cells, time-lapse movies were subjected to kymograph analysis in which line-scans of RhoA activity were plotted over time. In the control cells, RhoA activity remained restricted to a distinct "activity zone" at the leading edge, often with a peak of activity at the very cell edge (Figure 2B and Supplemental Movie S3A). This band of activity reflected high rates of ruffling and protrusive behavior in these regions. Indeed, there was a good correlation between membrane protrusions that were either actively growing or stable and the maintenance of high RhoA activity (Supplemental Figure S3). In contrast, although many GEF-H1–depleted cells displayed relatively higher levels of RhoA activity at the leading edge, they usually lacked the peak activity zone seen in the control cells. In addition, the RhoA activity in this region was not stable in the absence of GEF-H1 but displayed highly variable patterns with time (Figure 2B and Supplemental Movie S3B). Thus, depletion of GEF-H1 function in HeLa cells disrupted the persistent localization of active RhoA at the leading edge.

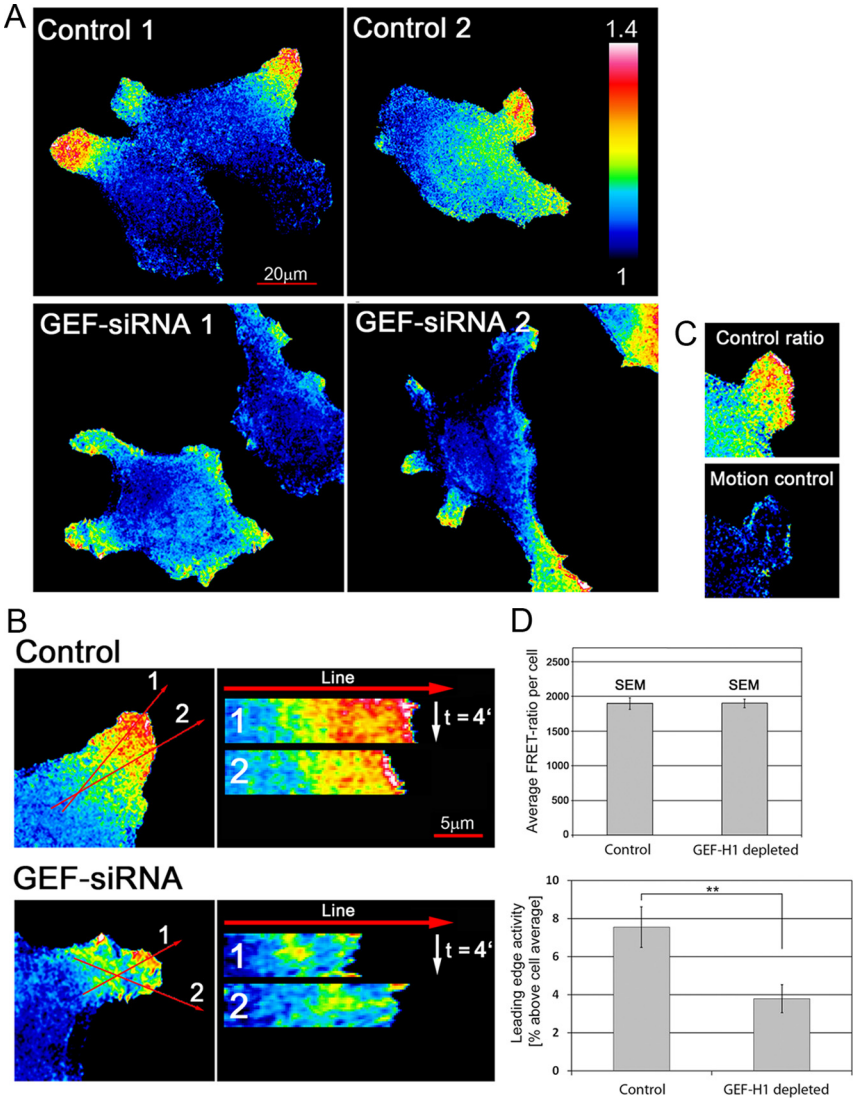

Figure 2. Depletion of GEF-H1 perturbs localized activation of RhoA at the edge of migrating HeLa cells. HeLa cells stably expressing a FRET biosensor for RhoA activity were transfected with control- and GEF-H1-siRNA, respectively, with >95% efficiency, and then cells selected at random for imaging. FRET ratio images denote activity patterns of RhoA under the conditions depicted. (A) Two representative pseudocolor images for localization of RhoA activity are shown for each condition. Bar, 20 μm. n = 18 control and 14 GEF-H1–depleted cells, respectively, from three independent experiments. (B) Localized RhoA activation in cell protrusions over time was assessed using time-lapse movies and kymographs. The first frame of representative movies is shown for cells with control and GEF-H1 siRNA. Kymographs were generated using ImageJ software with a bin-width of 1 and subjected afterward to an in-built Gaussian Blur Filter (σ radius = 1). Two typical kymographs per cell are shown (bar, 5 μm). The time-frame was 10 s for the duration of 4 min. (C) Motion control. False positive signals due to cell movement between the sequential CFP and FRET image acquisition. Three images were acquired: CFP-1, FRET, and CFP-2. Left, the actual ratio image was derived by dividing FRET by CFP-1. Right, the control image was obtained by dividing CFP-2 by CFP-1 to reveal maximum possible motion-related error. (D) Leading edge activity is decreased in cells depleted of GEF-H1. Top, average RhoA activation levels per cell were determined by measuring the average signal intensity of each ratio image with the built-in ImageJ "measure" tool. Results are means ± SEM from 34 (control) and 49 (GEF-H1–depleted) cells (n = 3 experiments). Bottom, RhoA activity in the leading edge relative to the cell average. A 1-μm-wide line was drawn along the border of each protrusion and average activity was measured within this region. Relative RhoA activity in the leading edge was calculated by division with overall average activity of the same cell. Only cells from time-lapse experiments were analyzed to focus on dynamic cell protrusions. Results are means ± SEM from 32 (control) and 33 (GEF-H1–depleted) cell protrusions with p value = 0.0047 (11 control and 10 GEF-H1 siRNA–treated cells).

GEF-H1 Depletion Alters Leading Edge Behavior during Cell Migration

Because of the loss of concentrated RhoA activity at the leading edge of randomly migrating cells, we wondered whether alterations of leading edge morphology might be associated with the depletion of GEF-H1, providing a possible underlying cause for defects in the motility of the cells. We used brightfield imaging and kymograph analysis of phase-contrast and DIC movies to assess the integrity and dynamics of control cells and GEF-H1–depleted HeLa cells (Figure 3 and Supplemental Movie S2). Control cells usually displayed a very characteristic and highly organized leading edge: individual small protrusions of routinely uniform size and appearance were extended, which subsequently converted into dense ruffles with a regular rearward flow. The distance covered by each ruffle during the inward flow was relatively steady, leading to a highly regular appearance of the kymograph (Figure 3A, control kymograph). In contrast, the leading edge of GEF-H1–depleted cells was extremely disorganized: The membrane extensions seemed to be less regular than in control cells and were often extremely large (Figure 3A, GEF-H1 siRNA kymograph; and B). Based on these observations we quantified the percentage of cells with protrusions >2.5 μm. Significantly higher numbers of GEF-H1–depleted cells generated these large extensions compared with control cells (Figure 3C). In addition, the ruffling was more random than in control cells. Both effects were accompanied by a decreased persistency of the generated protrusions, which tended to collapse to the point of origin rather than adhere (Supplemental Movie S2, GEF-H1 depleted). This behavior was detected in 70.0 ± 2.6% of GEF-H1–depleted cells, whereas only 20.8 ± 8.3% of control cells exhibited disorganized ruffling (n = 3 experiments, with 73 control and 95 GEF-H1 siRNA-treated cells). Interestingly, we also noted that GEF-H1 depletion not only changed the dynamic behavior of the leading edge, but also increased the overall number of cells that displayed a ruffling phenotype (control, 66 ± 9.9% vs. GEF-H1 depleted, 91.4 ± 1.5). Specificity of this phenotype was confirmed by using each individual oligonucleotide included in the siRNA mix targeting

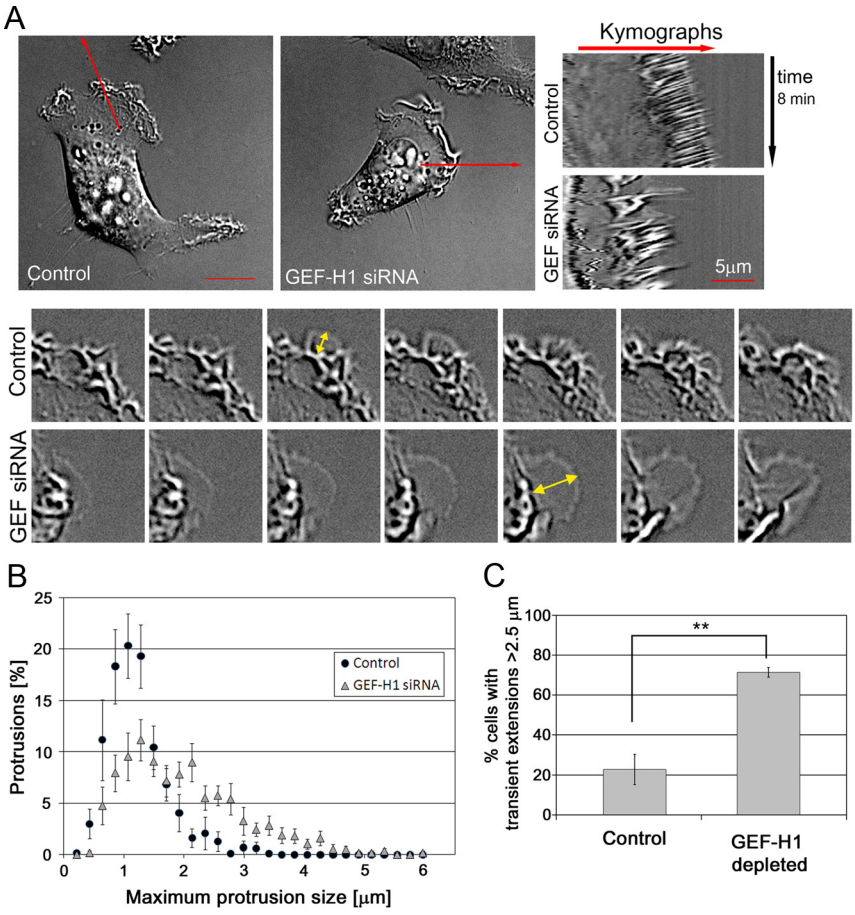

Figure 3. Dynamics of the leading edge is altered in GEF-H1 depleted cells. Cells were replated on glass coverslips 24 h post-siRNA transfection and subjected to time-lapse DIC microscopy at 72 h after transfection. Ruffling cells were chosen randomly for imaging purposes. Ruffling was defined by three-dimensional movement of the cell membrane inward from the leading edge. (A) Kymograph analysis of control- and GEF-H1–depleted cells. Left, representative images (first frame) of control- and GEF-H1–depleted cell movies. Bar, 10 μm. Right, representative kymographs. Kymographs of 73 control and 95 GEF-H1–depleted cells were generated using a built-in macro in MetaMorph software (n = 3 independent experiments). Frame rate, 5 s. The bottom two panels show a representative region of a control and GEF-H1–depleted cell, respectively. The maximum size of individual protrusions is indicated by yellow arrows. (B) Kymographs were used to measure maximum protrusion size during time-lapse recordings. n = 11 control and 10 GEF-H1–depleted cells from two independent experiments were analyzed. In total, 695 (control) and 602 (GEF-H1 siRNA) protrusions were measured. (C) Percentage of cells forming extensions >2.5 μm. Extensions were measured using the line tool. Each cell observed by time-lapse imaging was analyzed to avoid bias. Cells which formed neither ruffles, nor protrusions were neglected. Results are means ± SD of 76 control and 87 GEF-H1–depleted cells from three independent DIC time-lapse experiments. Significance between the two conditions was tested using *t* test analysis (**p < 0.01).

GEF-H1 (Supplemental Figure S4). This finding suggests that the molecular pathways necessary for initiation of protrusion and ruffle generation might be intact, albeit poorly controlled, in GEF-H1–depleted cells.

GEF-H1 Depletion Alters Dynamics of the Leading Edge Actin Cytoskeleton

We used fluorescence imaging to assess whether the effects on leading edge behavior observed when GEF-H1-RhoA signaling was perturbed were reflected by changes in the actin cytoskeleton. The most striking difference between control and GEF-H1–depleted cells regarding the actin cytoskeleton was the morphology and density of actin within the leading edge. Concomitant with the brightfield studies (Figure 3), the leading edge of control cells was well defined and contained a very dense population of actin rich membrane ruffles (Figure 4, A and B). The width of this F-actin–enriched area was relatively constant along the entire protrusion. In contrast, cells lacking the RhoA GEF displayed a nonuniform, irregular actin staining, in which the actin-rich ruffles were neither densely packed, nor continuous along the leading edge as in control cells (Figure 4, A and B, and Supplemental Figure S5). Interestingly, immunostaining with an antibody against GEF-H1 showed strong colocalization of endogenous GEF-H1 with F-actin in the ruffling membrane protrusions of control cells, supporting a potential regulatory role of GEF-H1 in the leading edge, presumably attenuating membrane ruffling (Figure 4C; also see Supplemental Figure S6 for confocal images).

HeLa cells do not display very pronounced internal stress fibers compared with fibroblasts. However, there were distinct differences in the orientation of stress fibers between control and the GEF-H1–depleted condition. During wound healing, control cells often displayed hemi-circumferential actin bundles which were localized in parallel to the leading edge and only visible at low focus (Figure 4D, control). In contrast to the controls, GEF-H1–depleted cells rarely displayed ordered actin bundles (Figure D, GEF-H1 depleted). Both in wound healing experiments and in single migrating cells, stress fibers were sparse and seemed randomly organized in cells lacking GEF-H1, without a preferential orientation with respect to the leading edge (Figure 4, A and D, GEF-H1 siRNA).

The half-rings observed in the control cells were reminiscent of the "actin arcs" described by other groups in neuronal growth cones and fibroblasts (Figure 4D, control) (Heath, 1983; Schaefer *et al.*, 2002, 2008). The persistent flow of such actin arcs has been implicated in the dynamics and retrograde transport of MTs (Gupton *et al.*, 2002; Schaefer *et al.*, 2002, 2008). Time-lapse studies with control cells using EGFP-tagged actin indicated that these actin fibers might indeed derive from the leading edge and move rearward to align eventually with the stress fiber population already existent in the cell body (Figure 4E and Supplemental Movie S4). Thus, GEF-H1 depletion severely disrupted the actin cytoskeleton in HeLa cells, leading to a significant loss of F-actin organization both at the leading edge and toward the cell interior.

GEF-H1 Depletion Alters Organization of the Microtubule Cytoskeleton

We could not detect significant changes in the microtubule-organizing center orientation in GEF-H1–depleted cells, indicating that the diminished migration observed was not

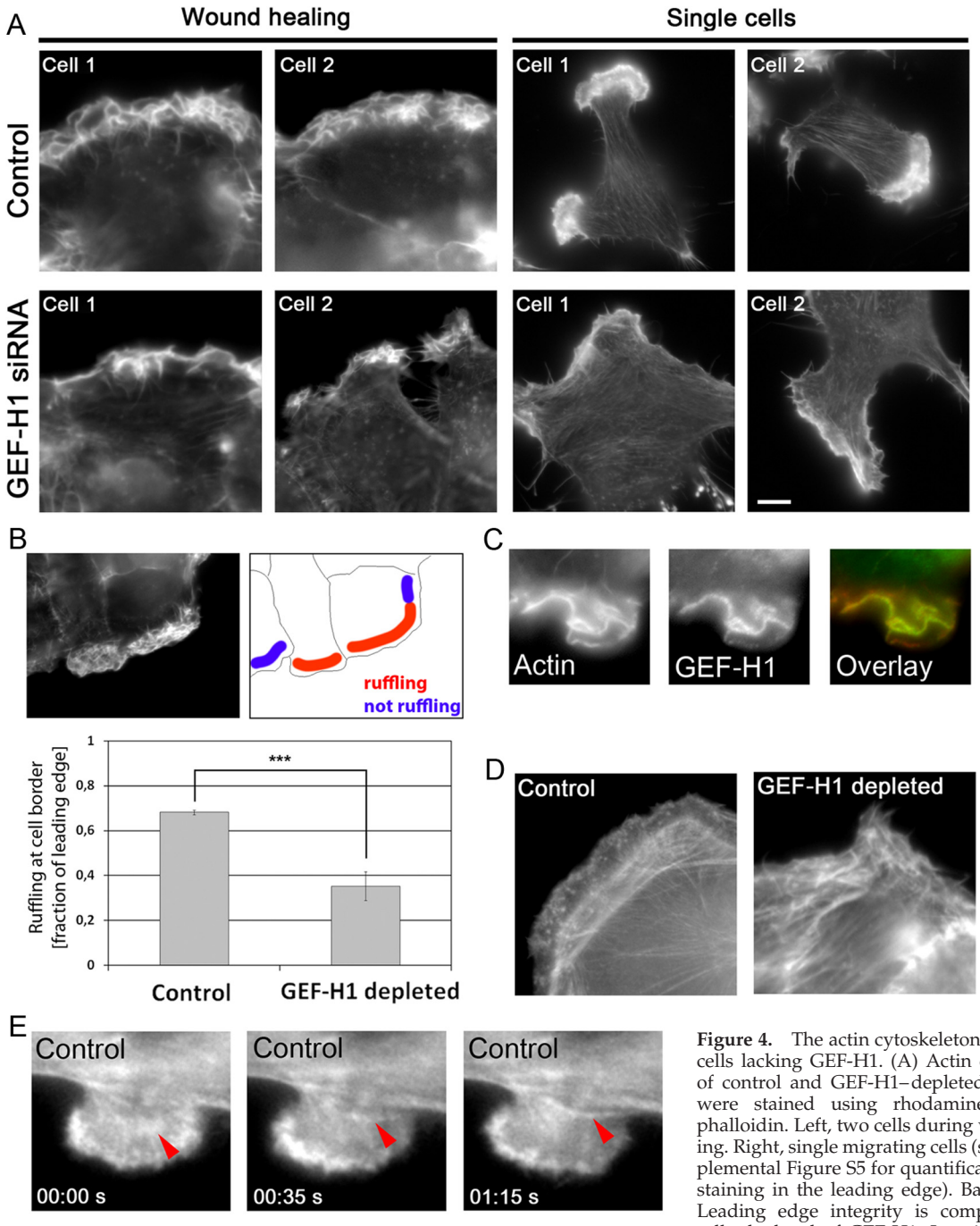

Figure 4. The actin cytoskeleton is altered in cells lacking GEF-H1. (A) Actin cytoskeleton of control and GEF-H1–depleted cells. Cells were stained using rhodamine-conjugated phalloidin. Left, two cells during wound healing. Right, single migrating cells (see also Supplemental Figure S5 for quantification of actin staining in the leading edge). Bar, 5 μm. (B) Leading edge integrity is compromised in cells depleted of GEF-H1. Imaging was performed along the wound at randomly chosen regions, and every cell in each image was analyzed. For each individual cell, the length of the entire leading edge region was measured using the line tool (ImageJ). In a second step, length of ruffling regions within the leading edge was measured (depicted in red in the schematic). Ruffling was defined as actin accumulation in a typically curled shape similar to three-dimensional membrane folds observed in DIC movies. "Ruffling at cell border" was calculated as fraction of the leading edge. Results are means ± SD of n = 2 independent experiments with 179 control and 232 GEF-H1–depleted cells. Statistical significance of the difference between the two conditions was assessed using *t* test analysis of all control versus GEF-H1–depleted cells ($p = 7.17\ e^{-11}$). (C) Colocalization of endogenous GEF-H1 and actin in membrane ruffles of migrating cells at the wound edge. (D) Stress fiber organization in the leading edge during wound healing. At low focus, actin fibers perpendicular to the cell edge were visible. (E) Example frames derived from the EGFP-actin movie of a control cell showing the formation of an actin bundle (red arrow) from an inward ruffling region (see also Supplemental Movie S4 and text). Frame rate, 5 s.

due to defects in cellular directionality (Supplemental Figure S7). However, we wondered whether in cells depleted of GEF-H1 the lack of transverse actin bundles would affect the organization and dynamics of the MT cytoskeleton. Anti-tubulin antibody staining of MTs showed that MTs were more densely packed at the cell edge in cells lacking GEF-H1 (Figure 5). In control cells the bulk of distinguishable MTs were present as an intertwined network often aligned par-

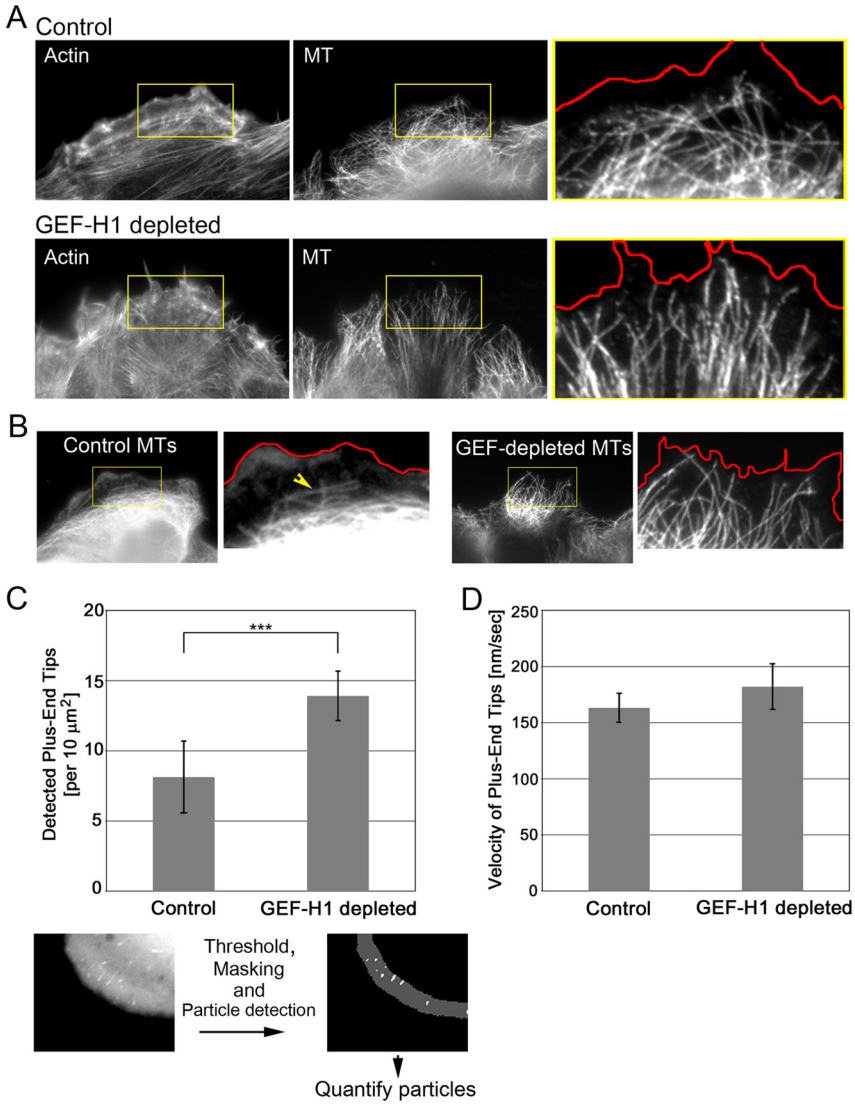

Figure 5. Microtubule organization is perturbed upon GEF-H1 depletion. (A) Costaining of the actin and the MT cytoskeleton. The figure shows cells migrating into the wound. Cells were fixed at 2 h after wound and stained with rhodamine-conjugated phalloidin and anti-α-tubulin antibody. To visualize the stress fibers, cells were imaged at low focus. A red line depicting the leading edge was generated based on the actin image and pasted onto the MT image to demonstrate the distance of MTs to the cell edge (enlarged box shown at right). (B) MT alignment with respect to the leading edge in migrating cells. Red line represents the actin boundary. (C) Quantification of MT tips approaching the leading edge. Cells were transfected with EGFP-EB-1 construct and subjected to fluorescence time-lapse imaging (frame rate, 5 s). The average number of EGFP-EB-1–decorated MT tips within a defined edge region was quantified as described in the bottom panels and in Supplemental Material. Results are means ± SD of four (control) and five (GEF-H1–depleted) cells, with each three analyzed regions. Statistical significance was assessed using Student's *t* test. $p = 0.0048$ (see also Supplemental Figure S9 for measurements with a significant number of fixed cells). (D) The velocity of EGFP-EB-1–decorated tips was measured using the Particle Tracker tool (ImageJ). Results are means ± SD of 196 (control) and 137 (GEF-H1–depleted) particles tracked in each five cells.

allel to, but localized in a considerable distance from, the leading edge (Figure 5A). This MT boundary region was defined by the arch-like parallel F-actin bundles present in the control cells (Figure 5A). In contrast, MTs in GEF-H1–depleted cells were oriented perpendicular to the cell edge and extended well into the leading edge area (Figure 5, A and B).

To measure the density of MT ends in the leading edge we performed time-lapse imaging of EGFP-EB1—the MT plus-end binding protein (Supplemental Movie S5) (Morrison *et al.*, 2002). Using the image analysis software ImageJ (http://rsb.info.gov/ij/), we quantified plus-end tips in the leading edge, determining the average number of plus-end tips ([per square micrometer, per frame]) within a defined region along the edge (for protocol, see Supplemental Figure S8 and Supplemental Movie S6). In GEF-H1–depleted cells, we observed a highly significant increase in the number of tips detected along the cell edge as compared with control conditions (Figure 5C). In addition, quantitation of MT density in the leading edge of fixed cells (Supplemental Figure S9) also showed a statistically significant difference between the two conditions.

To test whether MT growth was affected by GEF-H1 depletion as well, we tracked EGFP-EB1 particles for each time-point to determine the average tip velocity. Although there was a slight increase in GEF-H1–depleted cells, the difference in the velocity of MT tips between cells lacking the GEF and control cells was not significant (Figure 5D). Together, these observations suggest that GEF-H1 depletion impacts on MT behavior at the leading edge, perhaps resulting from deficient actin organization.

GEF-H1 Depletion Inhibits Focal Adhesion Turnover

RhoA signaling has been shown to regulate FA dynamics in various cellular systems (for reviews, see Ridley, 2001; Etienne-Manneville and Hall, 2002; Kaverina *et al.*, 2002). In particular, growth and maturation of focal complexes is driven by mechanical force generated by the actin- and myosin-containing contractile stress fibers (for review, see Bershadsky *et al.*, 2003). As shown in Figures 4 and 5A, stress fiber alignment during cell migration is aberrant in GEF-H1–depleted cells, and we showed previously that RhoA/ROCK-dependent phosphorylation of myosin II is inhibited in nocodazole-treated GEF-H1–deficient cells (Chang *et al.*, 2008). Brightfield analysis of migrating cells revealed that cells lacking GEF-H1 formed large protrusions at the leading edge (Figure 2 and Supplemental Movie S2) that often failed to adhere; instead, they folded back and gave rise to a large

ruffle. This observation suggested that aberrant RhoA activation at the leading edge might lead to defects in cell-substrate adhesion in the absence of GEF-H1.

We initially assessed FA organization by examining the FA-associated protein paxillin. Small focal complex-like structures were detected in the leading edge of control migrating cells (Figure 6A, enlarged box; and Supplemental Movies S8 and S9A). Behind this region and under the cell body, we detected larger FAs of varying size that were often associated with actin stress fibers. In contrast, the general appearance of the FAs differed in the GEF-H1–depleted cells: first, the leading edge rarely displayed focal complexes (Figure 6A, enlarged box). Second, we often noted an increased number of large FAs in the body of GEF-H1–depleted cells compared with control conditions (Figure 6A; data not shown). Overall, these observations suggested to us that FA turnover might be affected in cells lacking the GEF-H1–RhoA pathway.

We performed fluorescence live-cell imaging using EGFP-paxillin to assess FA dynamics. As seen in Figure 6B, the FAs in control cells matured and dissolved over the period of observation, whereas the adhesions in GEF-H1–depleted cells did not change their size over a long period (yellow arrows) (also see Supplemental Movie S7). To quantify the effect on FA dynamics, we used the IMARIS-Autoquant software (Bitplane, St. Paul, MN) to measure the FA turnover. This software allows the detection and tracking of FA in each frame of a time-lapse movie, as shown in Figure 6B, and can determine the period of time that each detected FA was visible in the movie. In the example shown in Figure 6C, small dots in gray represent the detected FA and the colored lines display the path of the FA during the movie. This analysis revealed that in GEF-H1–depleted cells the number of "long-lived" FAs was significantly increased, indicative of decreased turnover (Figure 6B, right).

As larger FAs were associated with the ends of acto-myosin–decorated stress fibers, we measured FA "sliding" by using the Image-Pro Plus software (MediaCybernetics, MediaCybernetics, Bethesda, MD). Using this analysis, we found that FAs in GEF-H1–depleted cells slide significantly slower throughout the duration of the experiment than in control cells, as reflected by the smaller slope of the colored lines (Figure 6D). This may mirror the reduced contractility of associated acto-myosin–based stress fibers.

A GEF-H1/RhoA/mDia Pathway Is Involved in Focal Adhesion Turnover

FA turnover has been shown to be regulated by a variety of mechanisms (for review, see Bershadsky *et al*., 2003). Contact of MT plus ends with peripheral FAs is one means of regulating their turnover (for review, see Small and Kaverina, 2003). However, we found that in GEF-H1–deficient cells there were greater numbers of MTs extending into the leading edge (Figure 5C), and we could detect no evident difference in their association with FA (data not shown). Similarly, the activity of p21-activated kinases (PAKs) has been shown to regulate FA lifetime and turnover (Manser *et al*., 1997). We could detect no differences in the levels of phosphorylated active PAK1/2 between control and GEF-H1–depleted cells (Supplemental Figure S10).

Tyrosine phosphorylation of FAK occurs during generation of FAs (for review, see Schlaepfer *et al*., 1999). Phosphorylation of FAK Tyr397 is not only important for FA assembly but also for their turnover during cell migration (Webb *et al*., 2004; Hamadi *et al*., 2005). Western blot analysis of control and GEF-H1–depleted cells revealed that there was a substantial decrease in FAK Tyr397 phosphorylation in cells lacking GEF-H1, concomitant with the decreased turnover of FAs (Figure 7A).

The RhoA effector mDia is involved in the recruitment of Src kinase to focal adhesions and its activation by FAK (Yamana *et al*., 2006). We therefore tested whether this effector might play a role in cellular effects observed upon depletion of GEF-H1. Using siRNA technology, we depleted mDia1 protein in HeLa cells and assessed phosphorylation of FAK Tyr397: Tyr397 phosphorylation was comparably decreased in cells lacking mDia1, implicating a possible involvement of this RhoA effector in the phenomena observed when GEF-H1 is lacking (Figure 7B).

The phosphorylation of FAK at the Tyr397 site is prerequisite for tyrosine phosphorylation of the downstream FA adaptor protein paxillin (Schaller and Parsons, 1995). Immunoprecipitation of paxillin and subsequent Western blot analysis with a tyrosine-specific antibody showed that there was indeed a strong decrease of paxillin tyrosine phosphorylation in cells lacking GEF-H1 (Figure 7C). Together, depletion of the Rho GEF, GEF-H1, strongly impairs the turnover of focal adhesions by perturbing tyrosine phosphorylation of key FA proteins, possibly due to the lack of proper RhoA effector signaling.

DISCUSSION

GEF-H1 Regulates RhoA Activity at the Leading Edge

During cell migration, RhoA GTPase activity regulates the actin cytoskeleton to efficiently coordinate leading edge protrusiveness and contractility of the cell body. Recent studies have detected a major region of RhoA activation at the front of migrating fibroblasts, reflecting such critical roles (Kurokawa and Matsuda, 2005; Pertz *et al*., 2006). Indeed, RhoA activation in this region temporally correlates with edge advancement (Machacek *et al*., 2009). However, it is still unknown how such localized RhoA activation is achieved by upstream mechanisms.

In the current study, visualization of RhoA activity with a live cell biosensor showed that GEF-H1 is a major regulator of localized RhoA activation in the leading edge of migrating HeLa cells. In contrast to the effects on localized activity, the overall RhoA activation level in cells was not significantly altered, as measured either by glutathione transferase-Rhotekin affinity-based assay (Chang *et al*., 2008) or by FRET (Supplemental Figure S3A). GEF-H1 thus controls the localized activation dynamics of the RhoA pool at the front of the migrating cell, rather than bulk RhoA activity. In agreement with this finding, we had recently shown that GEF-H1, acting in concert with Ect2, can regulate localized RhoA activation at the cleavage furrow during cytokinesis (Birkenfeld *et al*., 2007).

The role of the RhoA activity zone in the leading edge is still under investigation, but regulatory functions during cell migration are likely. Machacek *et al*. (2009) found a strict spatiotemporal correlation between RhoA, Rac1, and Cdc42 GTPases in the leading edge of migrating mouse embryo fibroblasts. In their study, RhoA was consistently activated first with respect to expansion of the protrusion, before Rac1 and Cdc42, suggesting a potentially dominant role for RhoA in initiating protrusion. In MTln3 cancer cells, EGF-induced leading edge RhoA activity was also found to function upstream of Rac1 and Cdc42 activation to regulate cell motility and actin dynamics in the leading edge (El-Sibai *et al*., 2008). Here, RhoA activity critically modulated protrusion size during MTln3 cell migration, with inhibition of RhoA causing an increase in basal cell area and formation of large,

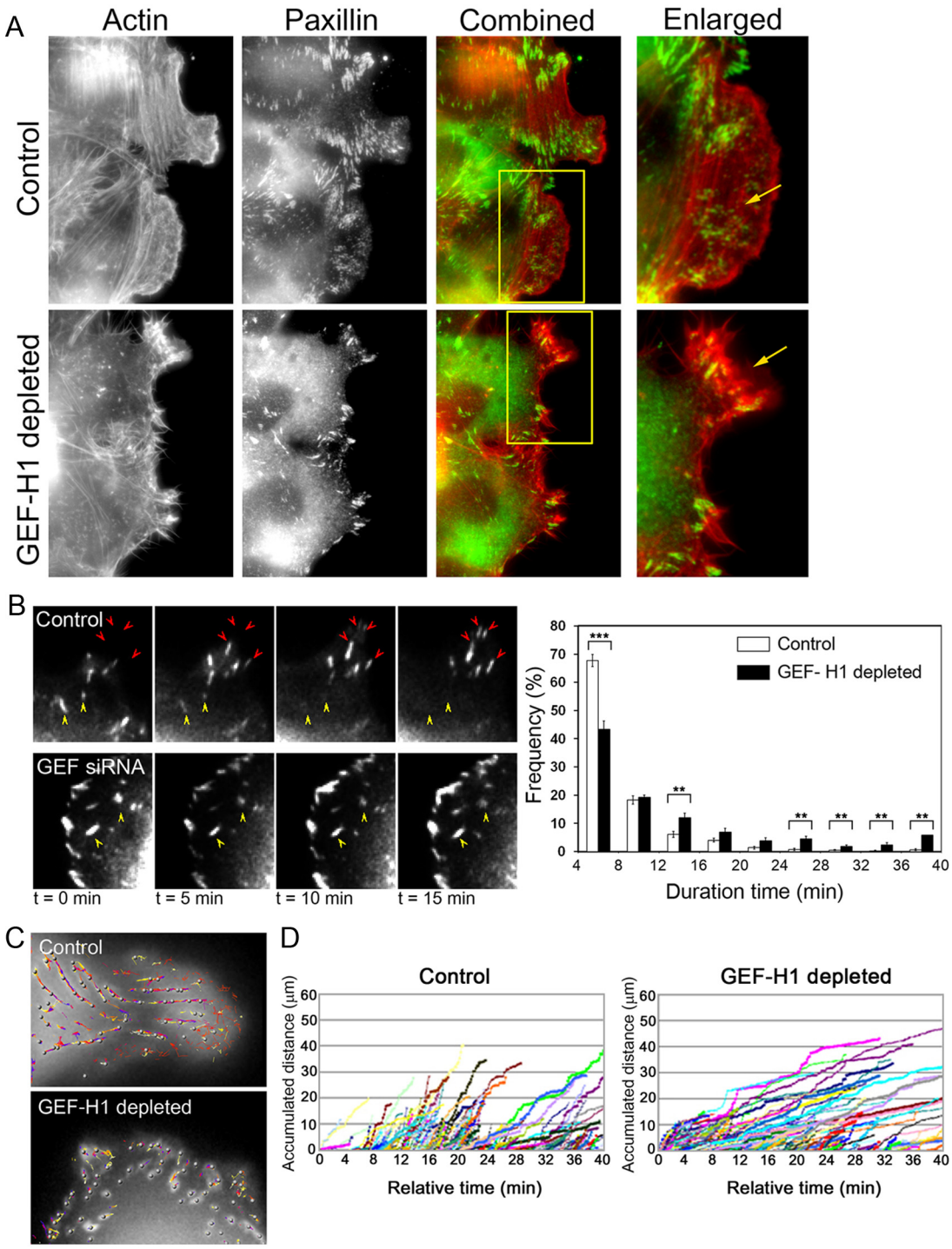

Figure 6. Turnover of focal adhesions is perturbed in GEF-H1-depleted cells. (A) Control or GEF-H1–depleted cells were fixed 2 h after wound and immunostained using antibody for paxillin together with rhodamine-labeled phalloidin. Arrow in enlarged control image indicates small focal complexes in the leading edge, whereas the arrow in the GEF-H1 siRNA-treated cell points to an extension deficient in paxillin-containing foci. (B) Left, representative EGFP-paxillin time-lapse images showing generation (red arrows) and dissolution (yellow arrows) of focal adhesions (see also Supplemental Movie S7). Right, frequency (percentage) of detected focal adhesions with the indicated "live-time" (detection duration). Particles were detected with IMARIS 5.0 software (Bitplane) and analyzed using Excel software (Microsoft, Redmond, WA). Binning, 4 min. Results are means ± SE of 10 regions in five control cells and 12 regions in six GEF-H1–depleted cells. Significance between the two conditions was tested for each time range. $p < 0.05$, $^{**}p < 0.01$, and $^{***}p < 0.001$. (C) Focal adhesion sliding in GEF-H1–depleted cells is slower than in control cells. Time-lapse videos of EGFP-paxillin–expressing cells were recorded for 40 min and analyzed to track EGFP-paxillin containing focal adhesions by IMARIS 5.0. Representative snapshots: gray dots show detected EGFP-paxillin foci. Colored lines display the tracked path of each dot during the time-lapse experiment. (D) Accumulated distance of tracked focal adhesion dots as measured using Image-Pro Plus software. Figures show representative analyses in which the slope is indicative of the speed of the detected adhesion point. Each colored line represents a detected and traced focal adhesion.

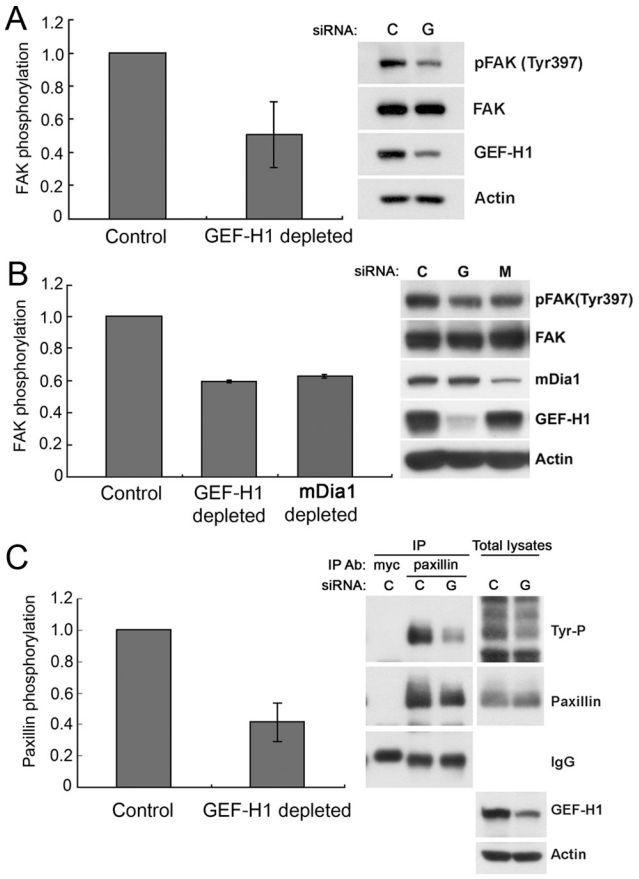

Figure 7. Tyrosine phosphorylation of focal adhesion components is altered in cells lacking GEF-H1. (A) Tyrosine phosphorylation of focal adhesion kinase is decreased in cells lacking GEF-H1. Cell lysates of control and GEF-H1–depleted cells were collected and examined by immunoblot for pFAK(Y397) and total FAK. For quantification, phosphorylated FAK was normalized to the amount of total FAK from whole cell lysates. Results are from n = 3 independent experiments, means ± SD. (B) Depletion of mDia1 leads to decreased FAK tyrosine phosphorylation during in vitro wound healing. Cells were transfected with control, GEF-H1 or mDia1 siRNA. At 72 h post-siRNA transfection, multiple scratch wounds were generated (18/3.5-cm dish), and cells were allowed to migrate for 6 h. Protein samples were collected and subjected to immunoblotting for pFAK(Y397) and total FAK. Left, quantification of pFAK(Y397) normalized to total FAK protein. Results are from n = 2 independent experiments, means ± SD (C) Tyrosine phosphorylation of paxillin is decreased in GEF-H1–depleted cells. Cell lysates of control and GEF-H1–depleted cells were IPed by using anti-paxillin antibody. Immunoprecipitates and total cell lysates were separated by SDS-PAGE and subjected to immunoblotting with the anti-phospho-tyrosine antibody 4G10 (Tyr-P). The membrane was stripped and reprobed with anti-paxillin antibody. Left, relative quantification of phospho-tyrosine paxillin to total paxillin from two independent IP experiments (means ± SD).

randomly oriented protrusions. These findings also support a critical role for RhoA in the tight balance between extension and contraction in order to achieve efficient cell migration.

The present data suggest a key role of GEF-H1–regulated RhoA activity in leading edge cytoskeletal regulation. Our time-lapse analysis of single migrating cells revealed strongly perturbed leading edge dynamics upon depletion of GEF-H1. In control cells GEF-H1 was found to accumulate in membrane ruffles within this region, consistent with a localized GEF-H1-RhoA signaling pathway (Figure 4C and Supplemental Figure S6).

GEF-H1 Regulates Cell Migration

As a consequence of unstable RhoA activity in the leading edge, the siRNA-mediated depletion of GEF-H1 led to a decrease in HeLa cell migration efficiency. Migration was inhibited to a similar extent in both a two-dimensional wounding assay and in a three-dimensional (3D) filter assay, suggesting similar GEF-H1 function in both types of cell migration. As single cells were used to study migration in 3D, aberrant regulation of cell–cell contacts is unlikely to explain our findings. Indeed, we could not detect significant alterations of cell-cell contacts in cells lacking GEF-H1 in in vitro scratch assays (Supplemental Figure S11). In contrast, our studies revealed multiple other migration-related cellular perturbations upon GEF-H1 depletion.

The aberrant leading edge dynamics in cells lacking GEF-H1 strongly correlated with alterations in the organization of the actin cytoskeleton at the cell edge. Both centripetal flow of leading edge ruffles and the spatial alignment of stress fibers were perturbed in the absence of GEF-H1. In control cells, we observed a distinct zone behind the leading edge in which curved actin bundles were aligned parallel to the cell boundary; such ordered actin structures were rarely detected in the absence of GEF-H1. In time-lapse studies with control cells, we were able to observe actin bundle generation associated with the rearward flow of actin from the leading edge. Transverse actin bundles, also termed actin arcs, have been reported in multiple cell types (Heath, 1983; Schaefer *et al*., 2002; Hotulainen and Lappalainen, 2006) and have been implicated in controlling dynamics and retrograde transport of MTs (Schaefer *et al*., 2002). Similarly, in our study only few MTs were found extending into the leading edge of control cells, with most MTs localized just behind the region where transverse actin bundles were located. In that area, many MTs were bent and aligned parallel to the leading edge, suggesting that actin bundles in HeLa cells might also guide MTs and confine their spatial organization. In agreement with this, the lack of transverse actin fibers in GEF-H1–depleted cells was paralleled by a substantial increase in MTs extending outward to the cell edge. Our measurements of MT tip movement suggest that MT growth per se was not affected by depletion of GEF-H1. Rather, the orientation of MTs mostly perpendicular with respect to the cell edge support the hypothesis that GEF-H1 might facilitate the controlled approach of MTs to the leading edge by modulating the dynamics of guiding actin fibers.

The observed accumulation of MTs in the leading edge could account for the uncontrolled protrusion observed upon RhoA inhibition. As reported previously, dynamic MTs promote protrusion via the activation of Rac in the leading edge (Waterman-Storer *et al*., 1999; Wittmann *et al*., 2003, 2004), and the MT-mediated increase of Rac1 activity in the leading edge might be the underlying cause for enhanced protrusion. Our preliminary data indicate that the overall cellular levels of Rac1, as measured by p21-binding domain pull-down experiments, are not significantly increased after depletion of GEF-H1 (data not shown). In support of this, the overall levels of PAK phosphorylation, a downstream effector of Rac, are also unchanged (Supplemental Figure S10). Rather, inhibition of RhoA-dependent actin bundling might allow the enhanced localization of MTs in the leading edge, leading to localized increase of Rac activity. In future studies, it will be interesting to use in vivo activity biosensors to examine localized Rac activity patterns at the leading edge in a GEF-H1–depleted background.

Focal Adhesion Turnover Is Decreased in the Absence of Active GEF-H1

FAs provide a crucial link between the actin cytoskeleton and the substrate to enable efficient force generation and transmittance during cell migration (Hu *et al*., 2007). In turn, maturation of FAs has been shown to be altered by external mechanical force, indicative of mechanosensitive regulatory pathways (Riveline *et al*., 2001). The perturbed contractility observed in GEF-H1–depleted cells was paralleled by alterations in FA behavior (Figures 6 and 7). The overall numbers of focal adhesions did not seem to be decreased, suggesting that formation of FA per se was unaffected. This is consistent with another study where inhibition of GEF-H1 function (GEF-H1-DH mut) in mouse embryonic fibroblasts did not interfere with the generation of focal adhesions (Lim *et al*., 2008). Time-lapse movies in the present study showed that FAs grew slower in cells depleted of GEF-H1, suggesting that loss of RhoA-dependent contractility might perturb the FA maturation process. Consistent with this, there was a dramatic increase in the average focal adhesion lifetime (Figure 6B, right). We also observed a decrease in FA "sliding" in GEF-H1–depleted cells during migration, indicating reduced stress fiber contractility. Taken together, dysfunctional GEF-H1-RhoA signaling impairs FA turnover in migrating cells.

Decreased PAK activity did not seem to play a significant role in the observed aberrant FA turnover in cells depleted of GEF-H1 (Supplemental Figure S10). Tyrosine phosphorylation of key FA proteins has been associated with focal adhesion disassembly and efficient cell migration (Webb *et al*., 2004; Hamadi *et al*., 2005). In agreement, we observed significantly decreased tyrosine phosphorylation of FAK and paxillin in cells lacking GEF-H1 (Figure 7). Integrin-triggered auto-phosphorylation of FAK on Tyr397 is critical for FAK activation and leads to further maturation of FAs. In addition, Tyr397 of FAK is not only important for the maturation of FAs but is also involved in the mDia-dependent recruitment of active Src kinase to the adhesion complex site (Yamana *et al*., 2006). Src recruitment is inseparably linked to FAK activity. We found that depletion of mDia1 induced a substantial decrease in FAK Tyr397 phosphorylation, suggesting that the RhoA effector mDia might be involved in focal adhesion regulation through a FAK–Src signaling axis.

Downstream of FAK-Src signaling, paxillin phosphorylation at Tyr31 and Tyr118 is crucial for focal adhesion disassembly and efficient cell migration (Zaidel-Bar *et al*., 2007; for reviews, see Schoenwaelder and Burridge, 1999; Brown and Turner, 2004). We observed a significant decrease in the overall tyrosine phosphorylation of paxillin in cells lacking GEF-H1. Paxillin itself is implicated in the localization of Tyr397-phosphorylated FAK into focal adhesions, indicating a possible positive feedback loop between FAK and paxillin tyrosine phosphorylation. The RhoA effector mDia might be involved in this scenario as an integrating factor to link FAK, Src and paxillin signaling and facilitate proper focal adhesion turnover in migrating cells. Gupton *et al*. (2007) reported highly disorganized leading edge dynamics and abnormal generation of protrusions when mDia function was inhibited. Interestingly, the protrusions described in this study were similar to the phenotype observed in our GEF-H1 depletion studies. Another study by Riveline *et al*. (2001) revealed that local application of external force enhanced directional FA growth in an mDia-mediated manner. These reports are consistent with our data, and strongly support the conclusion that the observed effects of GEF-H1 depletion on FA dynamics and protrusion are due to aberrant RhoA signaling.

The localization of RhoA/mDia signaling might be mediated by targeted release of GEF-H1 protein from MTs at or in the close vicinity of FAs. Persistent targeting of FAs by MTs has been reported to promote FA disassembly (Kaverina *et al*., 1998, 1999). It was suggested that MTs release relaxation factors that are critical for the proper turn-over of FAs (Efimov *et al*., 2008). GEF-H1 has been shown to activate RhoA upon release from MTs and, together with data from our study, this suggests that GEF-H1 might mediate such localized regulation of RhoA function. For future studies it will be intriguing to visualize localized RhoA activation together with FA dynamics to assess spatiotemporal correlation during cell migration.

In summary, we have established GEF-H1 as a major regulator of localized leading edge RhoA signaling in migrating HeLa cells. Our data reveal a GEF-H1–dependent route for cytoskeletal reorganization and FA dynamics via leading edge RhoA activation. Future studies will establish the potential connection(s) between GEF-H1-RhoA signaling and the localized regulation of leading edge Rac1 and Cdc42 activity.

ACKNOWLEDGMENTS

We thank Dr. Leif Dehmelt for helpful discussions throughout the study and critical reading of the manuscript. The technical assistance of Bruce Fowler is appreciated. This work was supported by National Institutes of Health grant GM-39434 (to G.M.B.).

REFERENCES

Baudoin, J. P., Alvarez, C., Gaspar, P., and Métin, C. (2008). Nocodazole-induced changes in microtubule dynamics impair the morphology and directionality of migrating medial ganglionic eminence cells. Dev. Neurosci. *30*, 132–143.

Benais-Pont, G., Punn, A., Flores-Maldonado, C., Eckert, J., Raposo, G., Fleming, T. P., Cereijido, M., Balda, M. S., and Matter, K. (2003). Identification of a tight junction-associated guanine nucleotide exchange factor that activates Rho and regulates paracellular permeability. J. Cell Biol. *160*, 729–740.

Bershadsky, A. D., Balaban, N. Q., and Geiger, B. (2003). Adhesion-dependent cell mechanosensitivity. Annu. Rev. Cell Dev. Biol. *19*, 677–695.

Birkenfeld, J., Nalbant, P., Bohl, B. P., Pertz, O., Hahn, K. M., and Bokoch, G. M. (2007). GEF-H1 modulates localized RhoA activation during cytokinesis under the control of mitotic kinases. Dev. Cell. *12*, 699–712.

Brown, M. C., and Turner, C. E. (2004). Paxillin: adapting to change. Physiol. Rev. *84*, 1315–1339.

Chang, Y. C., Nalbant, P., Birkenfeld, J., Chang, Z. F., and Bokoch, G. M. (2008). GEF-H1 couples nocodazole-induced microtubule disassembly to cell contractility via RhoA. Mol. Biol. Cell *19*, 2147–2153.

Danowski, B. A. (1989). Fibroblast contractility and actin organization are stimulated by microtubule inhibitors. J. Cell Sci. *93*, 255–266.

Efimov, A., Schiefermeier, N., Grigoriev, I., Ohi, R., Brown, M. C., Turner, C. E., Small, J. V., and Kaverina, I. (2008). Paxillin-dependent stimulation of microtubule catastrophes at focal adhesion sites. J. Cell Sci. *121*, 196–204.

El-Sibai, M., Pertz, O., Pang, H., Yip, S. C., Lorenz, M., Symons, M., Condeelis, J. S., Hahn, K. M., and Backer, J. M. (2008). RhoA/ROCK-mediated switching between Cdc42- and Rac1-dependent protrusion in MTLn3 carcinoma cells. Exp. Cell Res. *314*, 1540–1552.

Enomoto, T. (1996). Microtubule disruption induces the formation of actin stress fibers and focal adhesions in cultured cells; possible involvement of the rho signal cascade. Cell Struct. Funct. *21*, 317–326.

Etienne-Manneville, S., and Hall, A. (2001). Integrin-mediated Cdc42 activation controls cell polarity in migrating astrocytes through PKCzeta. Cell *106*, 489–498.

Etienne-Manneville, S., and Hall, A. (2002). Rho GTPases in cell biology. Nature *420*, 629–635.

Etienne-Manneville, S. (2004). Actin and microtubules in cell motility: which one is in control? Traffic *5*, 470–477.

Fukata, Y., Oshiro, N., Kinoshita, N., Kawano, Y., Matsuoka, Y., Bennett, V., Matsuura, Y., and Kaibuchi, K. (1999). Phosphorylation of adducin by Rho-kinase plays crucial role in cell motility. J. Cell Biol. *145*, 347–361.

Gardiner, E. M., Pestonjamasp, K. N., Bohl, B. P., Chamberlain, C., Hahn, K. M., and Bokoch, G. M. (2002). Spatial and temporal analysis of Rac activation during live neutrophil chemotaxis. Curr. Biol. *12*, 2029–2034.

Gupton, S. L., Salmon, W. C., Waterman-Storer, C. M. (2002). Converging populations of f-actin promote breakage of associated microtubules to spatially regulate microtubule turnover in migrating cells. Curr. Biol. *12*, 1891–1899.

Gupton, S. L., Eisenmann, K., Alberts, A. S., Waterman-Storer, C. M. (2007). mDia2 regulates actin and focal adhesion dynamics and organization in the lamella for efficient epithelial cell migration. J. Cell Sci. *120*, 3475–3487.

Hall, A. (1998). Rho GTPases and the actin cytoskeleton. Science. *279*, 509–514.

Hamadi, A., Bouali, M., Dontenwill, M., Stoeckel, H., Takeda, K., and Philippe, R. (2005). Regulation of focal adhesion dynamics and disassembly by phosphorylation of FAK at tyrosine 397. J. Cell Sci. *118*, 4415–4425.

Heath, J. P. (1983). Direct evidence for microfilament-mediated capping of surface receptors on crawling fibroblasts. Nature *302*, 532–534.

Hotulainen, P., and Lappalainen, P. (2006). Stress fibers are generated by two distinct actin assembly mechanisms in motile cells. J. Cell Biol. *173*, 383–394.

Hu, K., Ji, L., Applegate, K. T., Danuser, G., and Waterman-Storer, C. M. (2007). Differential transmission of actin motion within focal adhesions. Science *315*, 111–115.

Kaverina, I., Rottner, K., and Small, J. V. (1998). Targeting, capture, and stabilization of microtubules at early focal adhesions. J. Cell Biol. *142*, 181–190.

Kaverina, I., Krylyshkina, O., and Small, J. V. (1999). Microtubule targeting of substrate contacts promotes their relaxation and dissociation. J. Cell Biol. *146*, 1033–1043.

Kaverina, I., Krylyshkina, O., and Small, J. V. (2002). Regulation of substrate adhesion dynamics during cell motility. Int. J. Biochem. Cell Biol. *34*, 746–761.

Kraynov, V. S., Chamberlain, C., Bokoch, G. M., Schwartz, M. A., Slabaugh, S., and Hahn, K. M. (2000). Localized Rac activation dynamics visualized in living cells. Science *290*, 333–337.

Krendel, M., Zenke, F. T., and Bokoch, G. M. (2002). Nucleotide exchange factor GEF-H1 mediates cross-talk between microtubules and the actin cytoskeleton. Nat. Cell Biol. *4*, 294–301.

Kurokawa, K., Itoh, R. E., Yoshizaki, H., Nakamura, Y. O., and Matsuda, M. (2004). Coactivation of Rac1 and Cdc42 at lamellipodia and membrane ruffles induced by epidermal growth factor. Mol. Biol. Cell *15*, 1003–1010.

Kurokawa, K., Nakamura, T., Aoki, K., and Matsuda, M. (2005). Mechanism and role of localized activation of Rho-family GTPases in growth factor-stimulated fibroblasts and neuronal cells. Biochem. Soc. Transact. *33*, 631–634.

Kurokawa, K., and Matsuda, M. (2005). Localized RhoA activation as a requirement for the induction of membrane ruffling. Mol. Biol. Cell *16*, 4294–4303.

Lim, Y., *et al*. (2008). PyK2 and FAK connections to p190Rho guanine nucleotide exchange factor regulate RhoA activity, focal adhesion formation and cell motility. J. Cell Biol. *180*, *187*, 203

Machacek, M., Hodgson, L., Welch, C., Elliot, H., Pertz, O., Nalbant, P., Abell, A., Johnson, G. L., Hahn, K. M., and Danuser, G. (2009). Coordination of Rho GTPase activities during cell protrusion. Nature (in press).

Manser, E., Huang, H. Y., Loo, T.-H., Chen, X.-Q., Dong, J.-M., Leung, T., and Lim, L. (1997). Expression of constitutively active alpha-Pak reveals effects of the kinase on actin and focal complexes. Mol. Cell. Biol. *17*, 1129–1143.

Matsumoto, Y., Tanaka, K., Harimaya, K., Nakatani, F., Matsuda, S., and Iwamoto, Y. (2001). Small GTP-binding protein, Rho, both increased and decreased cellular motility, activation of matrix metalloproteinase 2 and invasion of human osteosarcoma cells. Jpn. J. Cancer Res. *92*, 429–438.

Mikhailov, A., and Gundersen, G. G. (1998). Relationship between microtubule dynamics and lamellipodium formation revealed by direct imaging of microtubules in cells treated with nocodazole or Taxol. Cell Motil. Cytoskeleton *41*, 325–340.

Morrison, E. E., Moncur, P. M., and Askham, J. M. (2002). EB1 identifies sites of microtubule polymerization during neurite development. Brain Res. Mol. Brain Res. *98*, 145–152.

Nalbant, P., Hodgson, L., Kraynov, V., Toutchkine, A., and Hahn, K. M. (2004). Activation of endogenous Cdc42 visualized in living cells. Science *305*, 1615–1619.

Palazzo, A. F., Cook, T. A., Alberts, A. S., and Gundersen, G. G. (2001). mDia mediates Rho-regulated formation and orientation of stable microtubules. Nat. Cell Biol. *3*, 723–729.

Pertz, O., Hodgson, L., Klemke, R. L., and Hahn, K. M. (2006). Spatiotemporal dynamics of RhoA activity in migrating cells. Nature *440*, 1069–1072.

Ren, Y., Li, R., Zheng, Y., and Busch, H. (1998). Cloning and characterization of GEF-H1, a microtubule-associated guanine nucleotide exchange factor for Rac and Rho GTPases. J. Biol. Chem. *273*, 34954–34960.

Ridley, A. (2001). Rho GTPases and cell migration. J. Cell Sci. *114*, 2713–2722.

Ridley, A. J., Schwartz, M. A., Burridge, K., Firtel, R. A., Ginsberg, M. H., Borisy, G., Parsons, J. T., and Horwitz, A. R. (2003). Cell migration: integrating signals from front to back. Science *302*, 1704–1709.

Riveline, D., Zamir, E., Balaban, N. Q., Schwarz, U. S., Ishizaki, T., Narumiya, S., Kam, Z., Geiger, B., and Bershadsky, A. D. (2001). Focal contacts as mechanosensors: externally applied local mechanical force induces growth of focal contacts by and mDia-1 dependent and ROCK-independent mechanism. J. Cell Biol. *153*, 1175–1186.

Rossman, K. L., Der, C. L., and Sondek, J. (2005). GEF means go: turning on RHO GTPases with guanine nucleotide-exchange factors. Nat. Rev. Mol. Cell Biol. *6*, 167–180.

Schaefer, A. W., Kabir, N., and Forscher, P. (2002). Filopodia and actin arcs guide the assembly and transport of two populations of microtubules with unique dynamic parameters in neuronal growth cones. J. Cell Biol. *158*, 139–152.

Schaefer, A. W., Schoonderwoert, V. T., Ji, L., Mederios, N., Danuser, G., and Forscher, P. (2008). Coordination of actin filament and microtubule dynamics during neurite outgrowth. Dev. Cell. *15*, 146–162.

Schaller, M. D., and Parsons, J. T. (1995). pp125FAK-dependent tyrosine phosphorylation of Paxillin creates a high-affinity binding site for Crk. Mol. Cell. Biol. *15*, 2635–2645.

Schlaepfer, D. D., Hauck, C. R., and Sieg, D. J. (1999). Signaling through focal adhesion kinase. Prog. Biophys. Mol. Biol. *71*, 435–478.

Schoenwaelder, S. M., and Burridge, K. (1999). Bidirectional signalling between the cytoskeleton and integrins. Curr. Opin. Cell Biol. *11*, 274–286.

Small, J. V., and Kaverina, I. (2003). Microtubules meet substrate adhesions to arrange cell polarity. Curr. Opin. Cell Biol. *15*, 40–47.

Waterman-Storer, C. M., Worthylake, R. A., Liu, B. P., Burridge, K., and Salmon, E. D. (1999). Microtubule growth activated Rac1 to promote lamellipodial protrusion in fibroblasts. Nat. Cell Biol. *1*, 45–50.

Webb, D. J., Donais, K., Leanne, A. W., Thomas, S. M., and Turner, C. E. (2004). FAK-Src signalling through Paxillin, ERK and MLCK regulates adhesion disassembly. Nat. Cell Biol. *6*, 154–161.

Wittmann, T., Bokoch, G. M., and Waterman-Storer, C. M. (2003). Regulation of leading edge microtubule and actin dynamics downstream of Rac1. J. Cell Biol. *161*, 845–851.

Wittmann, T., Bokoch, G. M., and Waterman-Storer, C. M. (2004). Regulation of microtubule destabilizing activity of Op18/stathmin downstream of Rac1. J. Biol. Chem. *279*, 6196–6203.

Wittmann, T., and Waterman-Storer, C. M. (2001). Cell motility: can Rho GTPases and microtubules point the way? J. Cell Sci. *114*, 3795–3803.

Worthylake, R. A., and Burridge, K. (2001). Leukocyte transendothelial migration: orchestrating the underlying molecular machinery. Curr. Opin. Cell Biol. *13*, 569–577.

Yamana, N., *et al*. (2006). The Rho-mDia pathway regulates cell polarity and focal adhesion turnover in migrating cells through mobilizing Apc and c-Src. Mol. Cell. Biol. *26*, 6844–6858.

Zaidel-Bar, R., Milo, R., Kam, Z., and Geiger, B. (2007). A paxillin tyrosine phosphorylation switch regulates the assembly and form of cell-matrix adhesions. J. Cell Sci. *120*, 137–148.

Zenke, F. T., Krendel, M., DerMardirossian, C., King, C. C., Bohl, B. P., and Bokoch, G. M. (2004). p21-activated kinase 1 phosphorylates and regulates 14–3-3 binding to GEF-H1, a microtubule-localized Rho exchange factor. J. Biol. Chem. *279*, 18392–18400.